ELSEVIER

International Journal of Mass Spectrometry 212 (2001) 25–40

International Journal of Mass Spectrometry

www.elsevier.com/locate/ijms

Design, optimization and initial performance of a toroidal rf ion trap mass spectrometer

Stephen A. Lammert[a,*], Wolfgang R. Plass[b,1], Cyril V. Thompson[a], Marcus B. Wise[a]

[a] *Chemical and Analytical Sciences Division, Oak Ridge National Laboratory, Oak Ridge, TN 37831-6365*
[b] *Department of Chemistry, Purdue University, W. Lafayette, IN 47907-1393*

Received 18 June 2001; accepted 30 July 2001

Abstract

The design, optimization, and initial performance of a novel ion trap mass analyzer is reported. This analyzer geometry is based on the edge rotation of an ion trap cross-section into the shape of a torus. The advantages of this design are that for a given device analyzer radius (r_0), significantly higher ion storage capacity than that obtained with a traditional three-dimensional quadrupole ion trap may be possible. Initial performance of this device was poor however, due to the significant contribution of additional nonlinear fields introduced by the rotation of the symmetrical ion trap cross-section. These nonlinear fields contributed to poor mass resolution and sensitivity as well as erratic ion ejection behavior. Using field analysis and ion trajectory simulation computer programs to guide the optimization, the geometry of this toroidal rf ion trap analyzer was modified in an attempt to correct for these nonlinear fields. These programs revealed that the original, symmetric toroid analyzer trapping field had a significant, sublinear component. Increasing the endcap separation and intentionally skewing the cross-sectional symmetry of the device minimized the field faults. Ion trajectory simulations indicated that the mass resolution and sensitivity of this asymmetric analyzer should be dramatically improved. Based on these results, an asymmetric version of the toroidal rf ion trap analyzer was constructed and this device has demonstrated unit mass resolution performance. (Int J Mass Spectrom 212 (2001) 25–40) © 2001 Elsevier Science B.V.

Keywords: Rf ion trap; Ion trap analyzer geometry; Geometry optimization; Simulations; Nonlinear fields; Ion storage

1. Introduction

Small analyzer size, simple ion optics, ultra high sensitivity, and the selectivity of MS^n are just a few of the reasons that ion trap mass spectrometry [1] has gained wide acceptance among mass spectrometry techniques. These same reasons have made ion traps the analyzer of choice for field portable applications [2–4]. While lab-based ion traps are on the small end of the range of mass spectrometer sizes, the size, weight, and power are determined to some extent by the large, resonantly tuned radio-frequency (rf) coil and power amplifier circuitry that provides the primary ion-trapping voltage. For a fixed ratio of analyzer axial (z_0) and radial (r_0) dimensions, the amplitude of the rf

* Corresponding author. E-mail: lammertsa@ornl.gov

[1] Current address: II. Physikalisches Institut, Justus-Liebig-Universität Giessen, Heinrich-Buff-Ring 16, 35392 Giessen, Germany

Dedicated to R. Graham Cooks on the occasion of his sixtieth birthday.

PII S1387-3806(01)00507-3

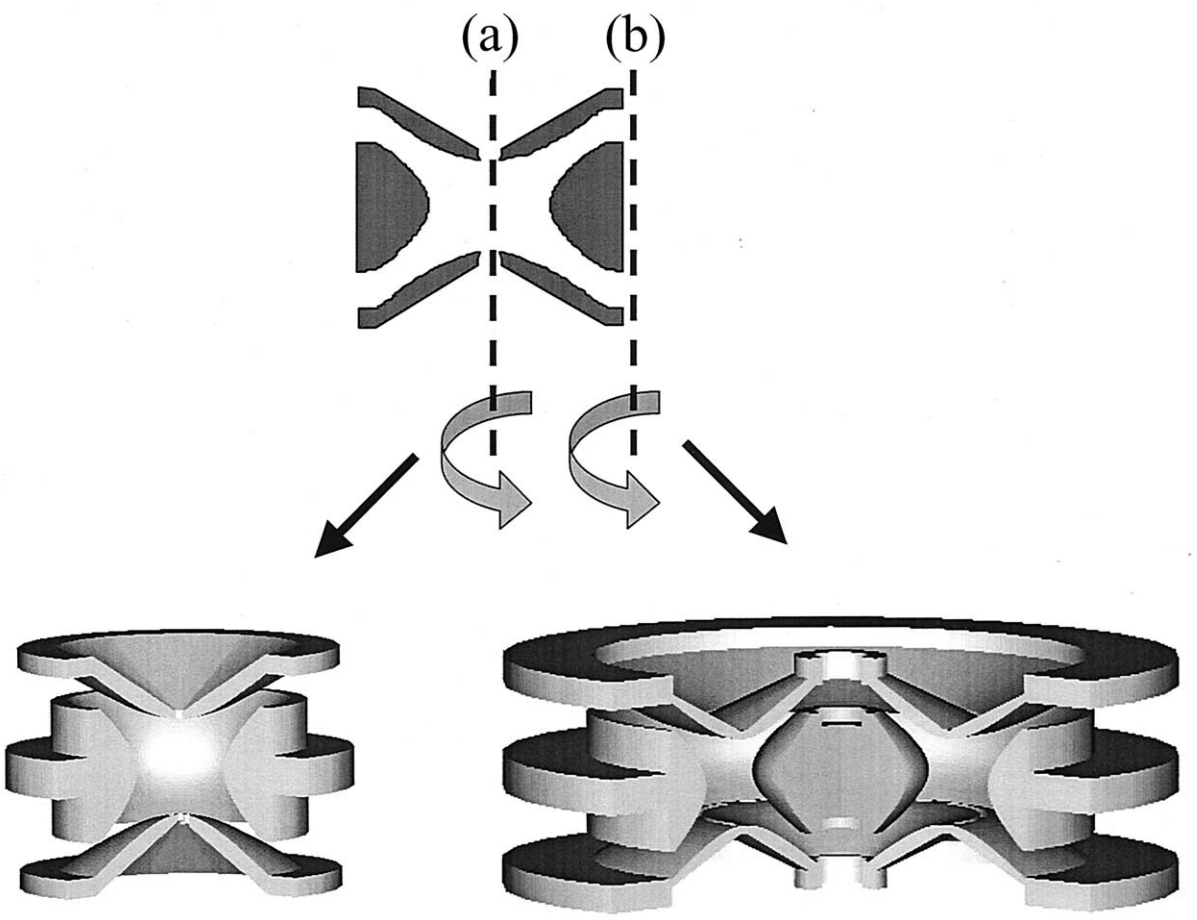

Fig. 1. The result of rotating a conventional 3D ion trap cross-section. Rotation on an axis that intersects at the intersection of the hyperbolae (a) gives the conventional 3D ion trap geometry. Rotation on an axis that is placed at some distance away from the intersection of the hyperbolae (b) gives a toroidal trapping geometry.

trapping voltage (V) is directly proportional to the square of the trapping field radius (r_0) as shown in

$$q_z = \frac{4eV}{m\ (\frac{1}{2}r_0^2 + z_0^2)\ \Omega^2} \tag{1}$$

where q_z is a Mathieu stability parameter, V is the amplitude of the radio-frequency (rf) trapping field voltage, m is the ion mass, r_0 and z_0 are the radial and axial dimensions, and Ω is the angular rf frequency. Equation (1) has recently been modified [5] to allow for any predominately quadrupole trap including more nontraditional geometries such as cylindrical ion traps [6].

$$q_z = -\frac{4eA_2V}{mr_N^2\Omega^2} \tag{2}$$

The A_2 term in Eq. (2) is the coefficient of the quadrupole term in the multipole expansion of the electric potential and reflects the strength of the quadrupolar field. The r_N term is the corresponding normalization radius. The relationship described by Eq. (2) offers an avenue for reductions in the rf power requirements as small reductions in the size of the ion trap analyzer lead to significant reductions in required rf trapping voltage for a given mass range. Unfortunately, smaller ion trap analyzers are more prone to the space charge performance degradation [7,8] that

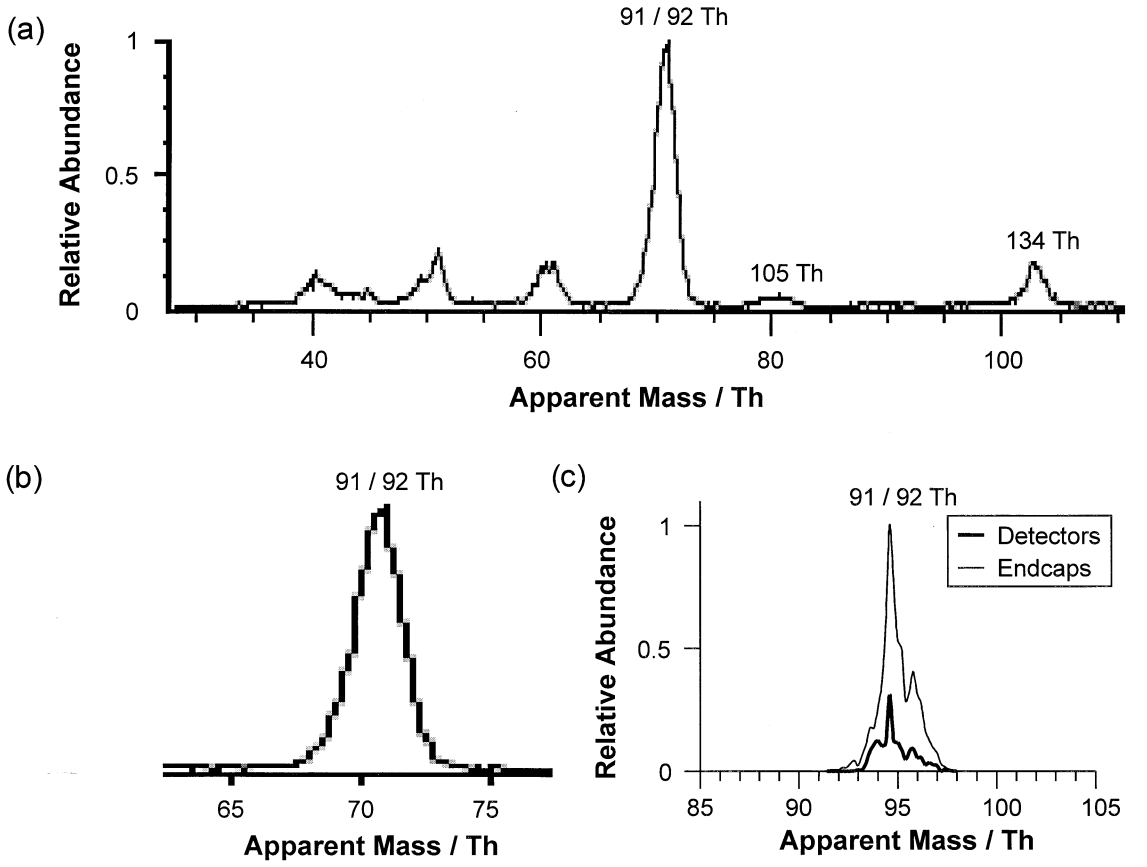

Fig. 2. Mass spectrum of n-butylbenzene obtained with the symmetric toroidal rf ion trap using resonance ejection at $\beta_z = 0.476$. The rf frequency ($\Omega/2\pi$) = 0.988 MHz, the applied resonance ejection signal $U_D = 12\ V_{p\text{-}p}$, the helium pressure = 4×10^{-5} mbar. (a) Experiment, (b) zoom of the mass peak at 91/92 Th, (c) simulation corresponding to (b). The mass scales for experiment and simulation are different, but the spectra cover the same actual mass range.

arises from ion-ion repulsion. Conversely, attempts to increase the ion storage capacity of laboratory-based ion trap mass spectrometers are limited by the squared relationship between analyzer size and trapping field rf amplitude. Current analytical ion trap mass spectrometers with a trap radius of approximately 1 cm have rf trapping voltages on the order of 15 $kV_{p\text{-}p}$. A further increase in trap dimensions would lead to significant increases in the already large amplitude rf voltage.

Recently, several groups [9–12] have investigated the use of linear quadrupoles as ion trapping devices. These devices take advantage of the fact that ions are forced to the center of the quadrupole assembly and are retained within the quadrupolar array by endplates held at elevated potentials. In a linear quadrupole trap the ion cloud is focused to a line rather than a point as in 3D quadrupole ion traps, allowing for an increased ion storage volume. The disadvantage of these devices is that they cannot be used for mass analysis as ions are dispersed throughout the length of the linear quadrupole structure. Bier and Syka reported [13] a solution for this problem by ejecting the ions through a slit in one of the rods onto a linear multichannel plate detector. In their patent, they proposed several variations of this design including one where they bent the linear quadrupole in such a way that the ions are ejected to a point, rather than a plane. The ejected

ions could then be detected by a continuous dynode electron multiplier. Another conceptual variation was described where the logical extension of this curved linear quadrupole led to a design that has the ends of the quadrupole meeting in a continuous circle. Dress and Paul [14] and Church [15] and others [16,17] have previously reported similar "racetrack" devices, but these have been used for ion storage experiments and not as a mass analyzer. Other precedence exists for curved quadrupoles in the form of the curved collision cell [18] on the Finnigan-MAT TSQ-70™ series and Quantum™ triple quadrupole mass spectrometers and the curved mass analyzers and collision cell in the early Bear Instruments (San Jose, CA) triple quadrupole systems [19]. While the purpose of these curved devices is not increased ion storage, they demonstrate that devices that rely on quadrupolar fields can accommodate distortions from their primary geometry and still function as intended. The distortion of the quadrupole trapping geometry introduces higher-order, nonlinear fields [20,21]. It should be noted that ion trapping devices with significant nonlinear fields can be successfully used for ion storage [22,23], but the mass analysis performance degrades dramatically [24] when even a small amount of unintended higher-order fields is present.

A new ion trap analyzer geometry has been conceived that is based on the edge rotation of the quadrupole ion trap cross-section as is shown in Fig. 1. As can be seen, the result of this edge rotation is a trapping field that is in the shape of a torus. While the conceptual origin of this device was independent and different, the resulting device is, in principal, similar in nature to the circular linear quadrupole reported by Bier and Syka in the above-cited patent. This toroidal rf ion trap design maintains a given trapping field radius while increasing the ion storage volume of the ion trap. Hemberger [25] has previously reported from ion tomography experiments that the collisionally cooled ion cloud occupies an approximately 1-mm-diameter sphere in the center of a conventional 3D ion trap analyzer. From a simple, strictly geometric argument the ion storage area would be roughly 240 times larger in a toroidal trap with the same cross-section radius (r_0) of 1 cm and an inscribed toroidal radius (R) of 2.54 cm.

Conversely, ion storage capacity comparable to that in a standard commercial 3D ion trap may be obtained in a significantly smaller radius toroid device. This would allow the operating rf voltage for the device to be reduced dramatically. Another possible advantage relates to a new degree of freedom for the ion motion (around the toroid) that may offer improvements in ion injection efficiency and ion activation [tandem mass spectrometry (MS/MS)] experiments.

As a proof-of-principle, an early version of the toroid analyzer was constructed based on the standard, stretched [24] ion trap cross-section of a Finnigan-MAT ITMS™ (San Jose, CA) ion trap mass analyzer. In this version, no attempt was made to correct for field imperfections that would be introduced from the rotation of the quadrupolar ion-trapping field, as no avenue to correct the fields was apparent at the time. Not surprisingly, the performance of this device was poor (vide infra) as split mass peaks, low signal intensity, and poor mass resolution characterized the spectra from this analyzer. In addition, the mass analysis performance was strongly dependent on the supplemental ac ejection beta-value used for the resonance ejection mass analysis scan. When the resonance ejection working point (β_z eject) was varied, peak splitting was observed at several values of β_z eject. For other values of β_z eject, the spectrum completely disappeared. The peak splitting and strong signal intensity dependence on the β_z-eject value suggest that field faults are the cause of poor performance in this device. This can be seen in Fig. 2(a), which shows the mass spectrum for n-butylbenzene using the symmetric toroid analyzer under optimized conditions. The spectrum was reproduced directly from the data system output and base peak in the spectrum is the unresolved mass pair at *m/z* 91 and *m/z* 92 as shown in detail in Fig. 2 (b). The mass scale in the figure does not correspond to the actual mass of the ions, as the current data system assumes the use of a conventional 3D ion trap using a resonance β-eject value of 0.958 (q eject equal to 0.906) and a rf trapping frequency ($\Omega/2\pi$) of 1.1

MHz. The current ITMS data system cannot accommodate changes in system calibration due to these nonstandard operating conditions. The unresolved *m/z* 91/92 peak splits into several peaks as the β-eject value is varied from optimized settings and for some values of β eject, the spectrum completely disappears.

As a result of these observations, a study was undertaken to evaluate and correct for the field faults introduced by the rotation of the quadrupolar trapping cross-section.

2. Theory

The theory [1,26] of quadrupole devices and their use as mass spectrometers is well covered in widely available texts. The electric potential in an ion trap with cylindrical symmetry can be expressed in terms of a multipole expansion, which in spherical coordinates (ρ,θ,ϕ) takes the form

$$\Phi(\rho,\theta,\phi,t) = \Phi_0\,(t)\sum_{l=0}^{\infty} A_l \left(\frac{\rho}{r_N}\right)^l P_l\,(\cos\,\theta) \qquad (3)$$

where Φ_0 is the electric potential applied to the ring electrode while the endcaps are grounded, r_N is a normalization radius that characterizes the size of the trap, A_l is the corresponding expansion coefficient of order l, and $P_l\,(\cos\,\theta)$ is the Legendre polynomial of order l. The monopole term ($l = 0$) does not contribute to the electric field and can be ignored. For ion traps with reflection symmetry with regard to the central plane the dipole term ($l = 1$) and all higher odd-order terms disappear. The quadrupole term ($l = 2$) constitutes the main contribution to the potential. In cylindrical coordinates (r,z) it is given by

$$\Phi(r,z,t) = \Phi_0\,(t)\,\frac{A_l}{r_N^2}\,(z^2 - \tfrac{1}{2}r^2) \qquad (4)$$

For purely quadrupolar devices, the corresponding fields are linear. Higher-order terms ($l > 2$) give rise to nonlinear fields. Although they are typically small compared to the quadrupolar field, they have been shown to be responsible for several important effects [21]. The oscillation frequency of the ions becomes dependent on the amplitude of the oscillation. This is particularly important during the final stage of the mass-selective instability scan. Negative, even higher-order fields have been shown to result in poor mass resolution and mass measurement accuracy [27,28]. Nonlinear fields also cause nonlinear resonance at certain working points in the stability diagram, resulting in unwanted ion loss [29]. However, nonlinear resonances can also be used advantageously during the mass-selective instability scan by applying a dipolar resonance voltage with a frequency that matches the nonlinear resonance. In the Bruker ESQUIRE™ (Bremen, Germany) commercial ion trap, this ejection method [30] is used at the hexapole resonance point ($\beta_z = 2/3$).

For this work, we will focus only on those aspects of quadrupolar devices as they relate to the toroid geometry. The form of a quadratic potential well with the minimum along a circle of radius R in the radial plane is given in cylindrical coordinates r and z by

$$\Phi\,(r,z) = \lambda\,(r - R)^2 + \mu\,z^2 \qquad (5)$$

The Laplace equation requires

$$\begin{aligned}\nabla^2\Phi &= 2\lambda\left(2 - \frac{R}{r}\right) + 2\mu \\ &= 2\lambda\left(2 - \frac{R}{R+s}\right) + 2\mu \\ &= 0\end{aligned} \qquad (6)$$

where λ and μ are arbitrary constants and

$$\mathrm{s} = \mathrm{r} - \mathrm{R} \qquad (7)$$

is the excursion from the potential minimum in the radial direction. Consequently, this potential distribution can be generated by electric fields only for the two cases

$$\mathrm{R} = 0 \qquad \text{(quadrupole ion trap)} \qquad (8)$$

$$\mathrm{R} \to \infty \qquad \text{(linear quadrupole)} \qquad (9)$$

Thus no toroidal rf ion trap with purely linear fields is possible. However, for $\mathrm{s} \ll \mathrm{R}$, i.e. for small excur-

sions from the potential minimum, nearly linear fields can be obtained. In this case, Eq. (3) reduces to

$$\lambda + \mu = 0 \tag{10}$$

In analogy with Eq. (4) the potential can then be written as

$$\Phi(s,z,t) = \Phi_0(t)\frac{A_2}{r_N^2}(z^2 - s^2) + \ldots \tag{11}$$

where $\Phi_0(t)$ is the electric potential on the ring electrodes, A_2 is a dimensionless coefficient, and r_N^2 is the corresponding normalization radius. The electric field components are

$$E_s = 2\Phi_0(t)\frac{A_2}{r_N^2}s \tag{12}$$

$$E_z = -2\Phi_0(t)\frac{A_2}{r_N^2}z \tag{13}$$

They are thus of the same absolute value and differ only in sign, like the fields in the linear quadrupole and unlike the fields in the quadrupole ion trap. Since it is the central fields that determine the onset of instability or resonance of cooled ion clouds, the ions will start to be ejected in radial and axial directions simultaneously, unless an additional quadrupolar dc potential is used to shift the ion oscillation frequencies or a dipolar resonance field is employed. When the ion oscillation amplitudes reach larger values, the nonlinear field contributions can modify the ejection process significantly. It is therefore necessary to optimize the toroidal analyzer geometry in order to reduce the nonlinear effects.

3. Methods

3.1. Field calculations and optimization

Commercial ion trap mass analyzers produce essentially linear quadrupolar trapping fields. A small, positive deviation from linearity is intentionally introduced by stretching the endcap distances (or modifying the asymptote angles as in the case of Bruker instruments) in order to improve mass analysis performance. It was assumed that in order to achieve similar mass analysis performance to that of commercial ion traps, the cross sectional trapping field of the toroidal analyzer should emulate this field. Due to the complication that the toroidal rf ion trap has to include slits in the electrodes to allow for the entrance and exit of electrons or ions, no attempt was made to optimize the electrode geometry analytically. Instead, the electric field was calculated numerically. The POISSON/SUPERFISH software package (Los Alamos National Laboratory, Los Alamos, NM) [31] was employed to calculate the electric potential. The program POISSON solves the Poisson equation by a successive over-relaxation method. In this work, a grid size of 0.1 mm was used for the discretization of the electrostatic problem. An external program was written that generates POISSON geometry input files for various ion trap geometries (including toroidal) of arbitrary dimensions, executes the POISSON programs, and extracts the potential values on a rectangular grid. The electric potentials are written to a potential array file that can be read and examined using the ion trap simulation program ITSIM (see Sec. 3.2.). The optimization was accomplished according to the following goals:

1. The ions should be able to leave the trap in the z direction through slits in the endcaps. This allows for easy detection of the ions in a plane.
2. A nearly linear electric field in the vicinity of $s = 0$ for any axial position inside the trap is required for good mass analysis performance, if ion ejection is to take place in the z direction. A small amount of positive higher-order fields in the region close to the inner circle of the torus field contribution should be included similarly as in commercial "stretched distance" or "modified asymptote" quadrupole ion traps.
3. A small radius of curvature (R/r_0) is necessary to allow for the eventual development of a reduced radius version.
4. The potential minimum should be located close to $s = 0$ for the ions to be ejected through the endcap slits located in the middle of the endcaps.

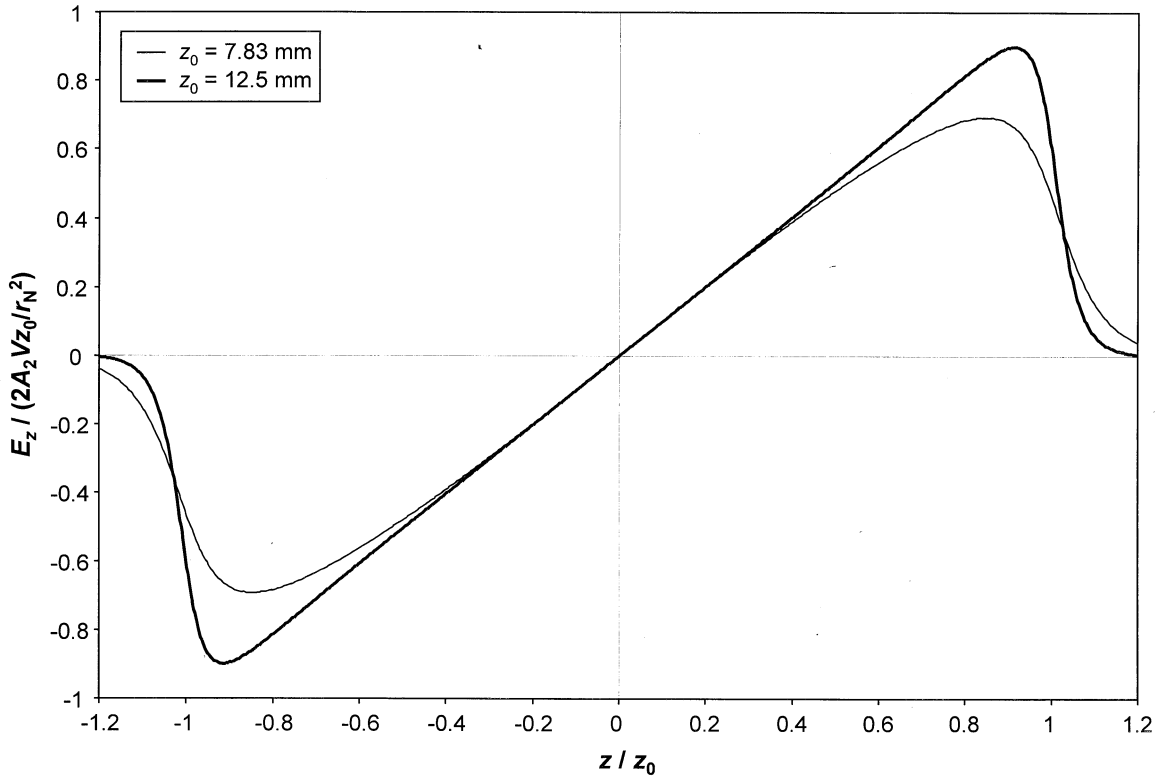

Fig. 3. Comparison of the axial electric field at $s = 0$ in the symmetric toroidal trap ($z_0 = 7.83$ mm) and the asymmetric toroidal trap ($z_0 = 12.5$ mm).

5. The nonlinear contributions to the radial field should be reduced as far as possible.

The endcap separation distance and the slope of the asymptotes of the electrode hyperbolae were chosen as the primary geometry parameters to be varied. Wang has previously demonstrated that adjusting the slope of the asymptote from the theoretical $1/\sqrt{2}$ allows the amount of additional nonlinear higher order fields to be modified [32]. Different values for the inner and outer ring electrode asymptotes were allowed to be separately changed to correct for the effects resulting from curvature. The resulting ring electrodes, however, maintained a symmetrical cross-section with respect to the radial center plane. The neighboring asymptote on each endcap was assigned to its counterpart on the corresponding ring asymptote, leading to an endcap geometry that is asymmetric from the outer ring electrode to the inner ring electrode. In addition, the distance of the endcap electrodes ($2z_0$) was allowed to be varied in order to correct for nonlinear field imperfections introduced by the entrance and exit slits. The slope of the inner ring electrode was varied from 0.7 to 1.9 with a resolution of 0.1 and the slope of the outer ring electrode from 0.7 to 1.2 with a resolution of 0.1. The endcap distance (z_0) was varied from 0.783 to 1.3 cm with a resolution of 0.05. Not all possible combinations were examined and the finest resolution steps were used only at values close to the optimum value.

3.2. ITSIM ion trajectory simulations

Simulations of mass scans for both geometries were performed using the ion trap trajectory simulation program ITSIM 5.0 (Purdue University, West

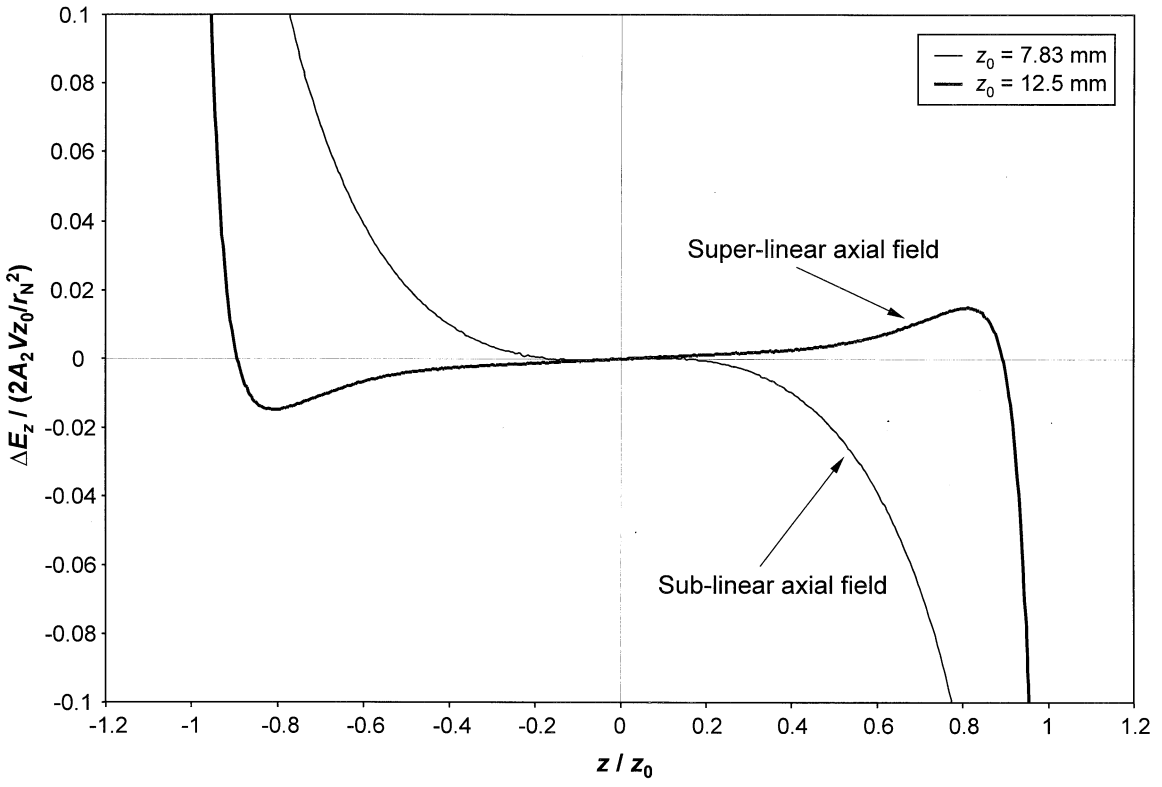

Fig. 4. Comparison of the nonlinear contributions to the axial electric field at $s = 0$ in the symmetric toroidal trap ($z_0 = 7.83$ mm) and the asymmetric toroidal trap ($z_0 = 12.5$ mm).

Lafayette, IN) [33–35]. ITSIM supports hyperbolic, cylindrical, and toroidal rf ion traps of arbitrary dimensions. The voltages are defined in the form of scan tables, similar to those used in early commercial ion traps. The rf, ac, and dc voltages as well as SWIFT and arbitrary waveforms can be applied in the monopolar, dipolar, and quadrupolar modes, allowing for simulation of virtually any scan function possible in real rf ion traps. The electric field is calculated either by interpolation from an array of precalculated electric potential values, or by a multipole expansion. The first method was used for the simulations shown here. The ion trajectories are calculated numerically by integration of Newton's equation of motion. A standard fourth-order Runge–Kutta method with a step size of 5 ns was used in this work. A collision model that takes into account velocity-dependent collision cross-sections allows for the treatment of elastic and inelastic collisions of the ions with the buffer gas and subsequent unimolecular dissociation of the ions. Here, only the elastic collision model was used, assuming Langevin collisions between the ions and the helium buffer gas. In addition to its trajectory calculation capabilities, ITSIM can also calculate and display electric fields from a precalculated potential file (such as POISSION).

The poor performance of the symmetric version of the toroid analyzer was observed in the simulation of the symmetric toroid analyzer using the ITSIM program under equivalent operating conditions. The simulated spectrum for *m/z* 91 and *m/z* 92 is shown in Fig. 2(c) for comparison to Fig. 2(b). The simulation predicts marginally better mass resolution than was obtained experimentally, however this can be explained by the fact that the simulation did not take space charge effects into consideration.

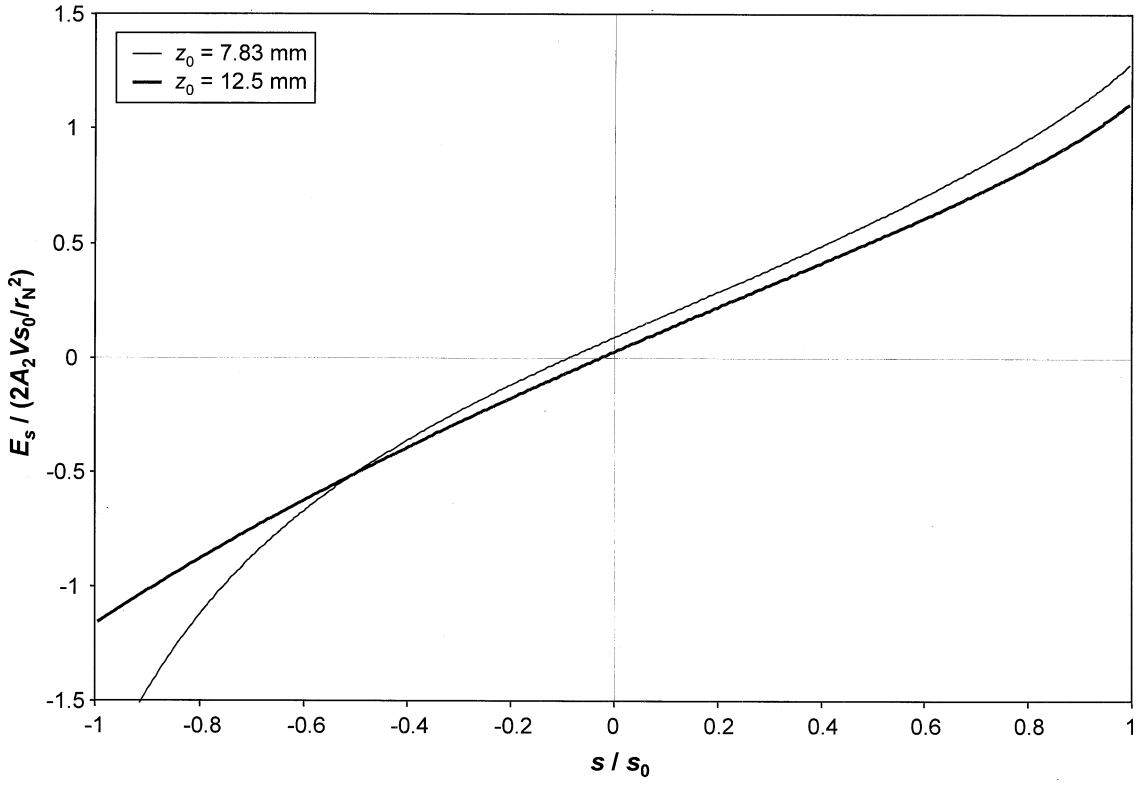

Fig. 5. Comparison of the radial electric field at $z = 0$ in the symmetric toroidal trap ($z_0 = 7.83$ mm) and the asymmetric toroidal trap ($z_0 = 12.5$ mm).

3.3. Fabrication and instrumental

The original toroid mass analyzer was designed by rotating the center point in the cross-section of a standard "stretched" ion trap [24,36] around a 2-in.-diameter circle. Slots were designed into the endcaps to replace the entry/exit holes found in standard ion trap cells. Four "bridges" over the slots were used to preserve the structural integrity of the endcaps. Tolerances of the machined parts were typically ± 0.003 in. or less. Hyperbolae on the endcaps and ring electrodes (inner and outer) were machined from the appropriate formulas using a CNC milling machine, with increments of less than 0.001 in. The asymmetric toroid mass analyzer was also designed with a 2-in.-diameter for the center of the analyzer and machining tolerances and conditions were the same as those for the symmetric version.

A custom Galileo (Sturbridge, MA) multichannel plate (MCP) detector was designed for use with the mass spectrometer, and a special mounting system was designed and fabricated. The custom MCP was fabricated at Galileo by removing a 25-mm-diameter center portion from a stock, 70 mm MCP detector. This same detector was used for both symmetric and asymmetric geometries with only slight differences in the mounting hardware. A filament assembly from the previously mentioned Finnigan-MAT ITMS™ was modified for use as a point ionization source for the analyzer. Separate filament assemblies were designed for each toroidal analyzer geometry to allow the ion source to be positioned on the back of the upper endcap in the recess of the hyperbola with the filament assembly aperture centered over the endcap slit.

The Finnigan ITMS™ ion trap system was modified for use as a test bed for the toroidal mass

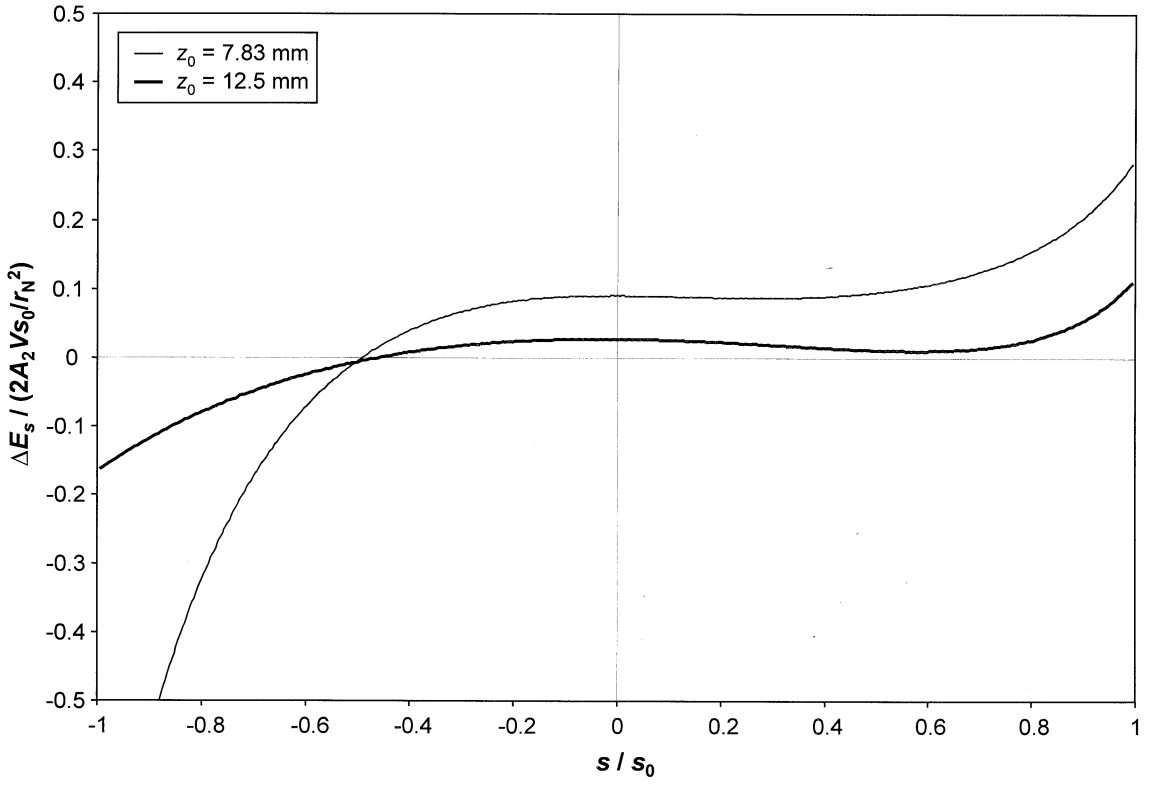

Fig. 6. Comparison of the nonlinear contributions to the radial electric field at $z = 0$ in the symmetric toroidal trap ($z_0 = 7.83$ mm) and the asymmetric toroidal trap ($z_0 = 12.5$ mm).

analyzer. The large vacuum chamber of the ITMS™ was replaced by a cylindrical, open top vacuum chamber with a diameter of 34 cm. By maintaining the analyzer radius (r_0) of the toroid rf ion trap at the same 1 cm value as the commercial ITMS™ ion trap, relatively few modifications were necessary to the control electronics. The ionization and detection circuits were directly compatible. The larger mass analyzer has a somewhat increased capacitance (approximately 34 pf for the symmetric toroid analyzer compared to approximately 25 pf for the ITMS™). This difference required the retapping of the ITMS™ primary rf transformer coil and the subsequent modification of the rf drive frequency. The modification of the rf drive frequency was accomplished by removing the 2200 kHz crystal oscillator from the rf control circuit on the ITMS Analog Board and injecting a variable frequency sine wave control signal from an Hewlett Packard (Palo Alto, CA) model 3325A Frequency Synthesizer/Function Generator into the rf drive circuitry ahead of the divide-by-two circuit. The rf drive frequency was subsequently tuned to minimize the reflected power for each of the toroidal

Table 1
Comparison of the figures of merit for the symmetric and asymmetric versions of the toroidal rf ion trap mass analyzer

	Symmetric geometry	Asymmetric geometry
Inner ring r_0 (cm)	1.0	1.0
Outer ring r_0 (cm)	1.0	1.0
Slope of the inner ring asymptote	0.707	1.8
Slope of the outer ring asymptote	0.707	0.7
Endcap distance (z_0) (cm)	0.783	1.25
Asymptote truncation	2.2 * r_0	2.2 * r_0
Entrance/exit slit diameter (mm)	1.78	1.5
rf drive frequency (kHz)	990	1038
R (cm)	2.54	2.54

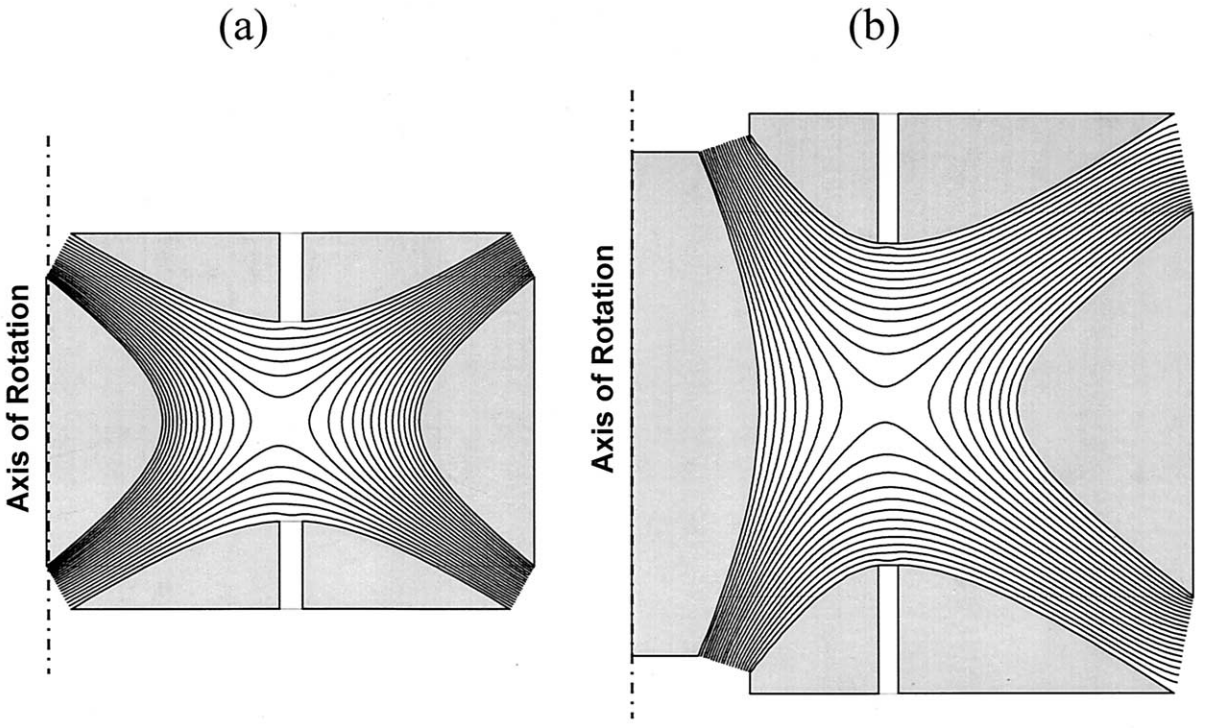

Fig. 7. Schematics of the electric potential distributions for the (a) symmetric toroidal trap and the (b) asymmetric toroidal trap.

analyzer geometries. The symmetric toroidal mass analyzer tuned at an rf frequency of approximately 990 kHz while the asymmetric version (due to a slightly different capacitance) tuned at a frequency of 1038 kHz. The tune value of 1038 kHz for the asymmetric toroidal analyzer was a fortuitous improvement as the 990 kHz tune point of the symmetric version was near the limits of the bandpass on the commercial ITMS™ rf electronics (which is centered on 1100 kHz). As such, it was difficult to achieve a full mass range under certain conditions in the symmetric toroidal analyzer.

Samples (n-butylbenzene, benzene, and perchloroethylene) as well as the helium buffer gas were introduced directly into the vacuum chamber using a leak valve (Granville-Phillips, Boulder, CO). Performance characteristics (mass resolution and signal intensity) were then monitored as a function of sample/helium pressure, ejection q value, and analyzer storage times.

4. Results and discussion

4.1. Field optimization using POISSON

The axial and radial fields of the two different toroidal analyzer versions were calculated as described above. The calculations used a radius of curvature (R) value of 2 cm, which is slightly smaller than the actual value of 2.54 cm used in both the symmetric and asymmetric analyzers. A calculation of the fields (data not shown) using the actual hardware dimensions used shows that the differences in the field are negligible for the purposes of this study. In fact, the radial field distortions should be somewhat better in the actual device than shown in the simulation, as the magnitude of analyzer curvature is less.

The axial fields (E_z, for the plane $s = 0$) of both the original symmetric geometry and the optimized asymmetric geometry are compared in Fig. 3. The two versions are delineated in the figure by their axial

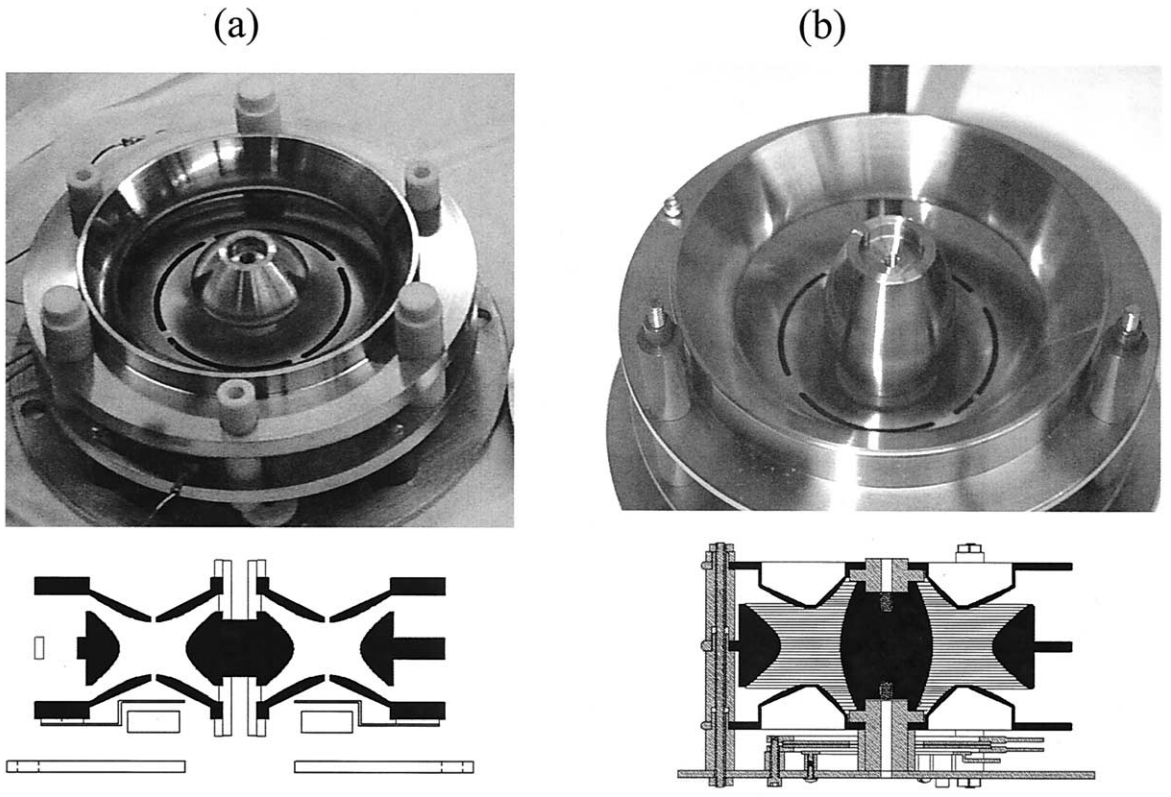

Fig. 8. Photographs (filament endcap removed) and line drawings of the analyzer components for the (a) symmetric toroidal trap and the (b) asymmetric toroidal trap.

dimensions; the symmetric toroidal analyzer has a $z_0 = 7.83$ mm and the asymmetric toroidal version has a $z_0 = 12.5$ mm. Fig. 4 compares the nonlinear contributions to the trapping field by subtracting a linear extrapolation of a narrow region of the derived electric field near the center of the trap (where the contributions due to nonlinear fields approach zero). The original geometry gives rise to a strongly sublinear axial field (the field deviates negatively from a projected linear field increase as a function of distance from the center of the trap) and the linearity is improved significantly, primarily by the stretch in endcap separation. A small superlinear contribution (the field deviates positively from a linear projection) was incorporated, similar in magnitude to that used in commercial "stretched geometry" quadrupole ion traps. The stretch of z_0 to more than $z_0 = s_0$ compensates for the effect of the endcap slits, which cause a decrease of the electric field strength (due to field penetration) in the vicinity of the slit. It was also determined by the simulations that reducing the width of the entrance/exit slits from the 1.78 (in the symmetric version) to 1.5 mm would reduce the nonlinear contribution from the slits while still allowing ions to efficiently exit the trap.

A disadvantage of the optimized geometry compared to the original geometry is the somewhat smaller field strength achieved in the asymmetric trap for a given rf amplitude. This leads to a smaller mass range. The coefficient A_2 was calculated for both geometries by a fit of Eqs. (12) and (13) to the electric field values in the central part of the trapping field. The coefficient for the original geometry is $A_2 = -0.564$ and the coefficient for the optimized geometry is $A_2 = -0.374$.

The optimized radial field (E_s, for the plane $z = 0$)

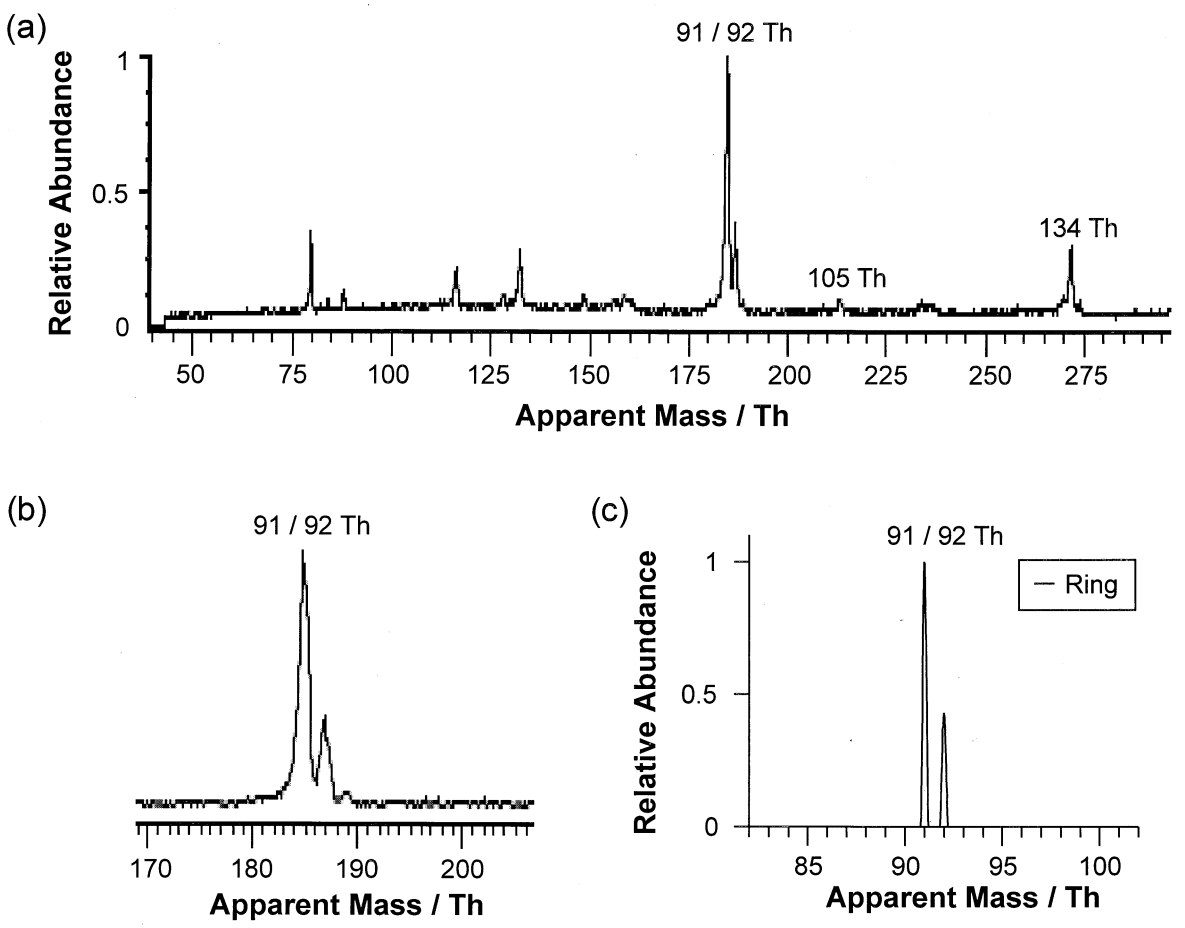

Fig. 9. Mass spectrum of n-butylbenzene obtained with the asymmetric toroidal rf ion trap using resonance ejection at $\beta_z = 0.666$. The rf frequency $(\Omega/2\pi) = 1.034$ MHz, the applied resonance ejection signal $U_D = 12$ $V_{p\text{-}p}$, the helium pressure $= 4 \times 10^{-5}$ mbar, the n-butylbenzene sample pressure $= 1 \times 10^{-7}$ mbar and the ionization time $= 75$ ms. (a) Experiment, (b) zoom of the mass peak at 91/92 Th, (c) simulation corresponding to (b). The mass scales for experiment and simulation are different, but the spectra cover the same actual mass range.

is shown in Fig. 5 and compared to the radial fields in the original symmetric toroidal trap. The nonlinear contribution in the two geometries (determined as above) is compared in Fig. 6. Clearly, nonlinear contributions to the radial field are still present in the optimized geometry, however they have been reduced. The surviving radial nonlinear fields are considerably less important to mass analysis than are those in the axial dimension as the ion cloud will be radially cooled prior to mass analysis. In summary, while the effects of changing the endcap distance cannot be completely uncoupled from the effects of changing the slope of the ring electrode asymptotes, the effects of increasing the endcap distance (z_0) can primarily be observed in the E_z plots (Figs. 3 and 4) as a transition from a sublinear condition to a slightly superlinear condition. The effects of asymmetrically changing the slope of the asymptotes can primarily be seen in the E_s plots (Figs. 5 and 6) in the form of decreased asymmetry.

The changes from the original to the optimized toroidal analyzer geometry are summarized in Table 1. A schematic comparing the potential distribution for the original symmetric version and the optimized

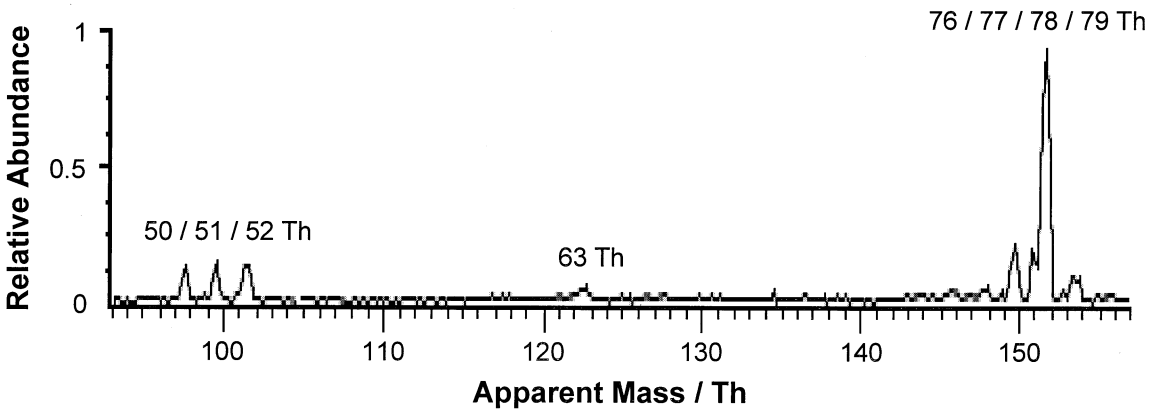

Fig. 10. Mass spectrum of benzene obtained with the asymmetric toroid trap using resonance ejection at $\beta_z = 0.666$. The rf frequency ($\Omega/2\pi$) = 1.034 MHz, the applied resonance ejection signal $U_D = 12\ V_{p\text{-}p}$, the helium pressure = 4×10^{-5} mbar, the benzene sample pressure = 2×10^{-7} mbar and the ionization time = 25 ms.

asymmetric version is shown in Figs. 7 (a) and 7 (b). The angle of the outer ring electrode asymptote was decreased (with respect to the radial plane) and the inner ring electrode asymptote was increased. The net effect was to decrease the absolute value of the electric field in the radial direction closest to the inner ring electrode. As a consequence, the minimum of the potential now lies at nearly the same radial position as the endcap slits as can be seen in Fig. 7 as well as in Fig. 5. The photographs and line drawings in Figs. 8 (a) and 8 (b) compares the symmetric and asymmetric toroidal mass analyzers.

4.2. Simulation and experimental results for the asymmetric toroidal rf ion trap

The predicted improvement from the original to the optimized geometry can be observed by comparing Fig. 9(c) with Fig. 2(c). The performance of the asymmetric version of the toroidal analyzer was

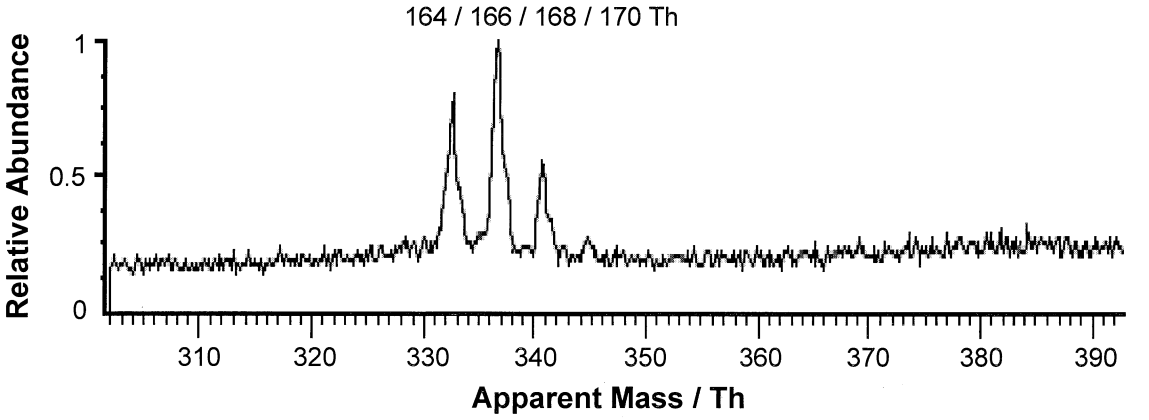

Fig. 11. Mass spectrum of perchloroethylene using resonance ejection at $\beta_z = 0.666$. The rf frequency ($\Omega/2\pi$) = 1.034 MHz, the applied resonance ejection signal $U_D = 12\ V_{p\text{-}p}$, the helium pressure = 4×10^{-5} mbar, the perchloroethylene sample pressure = 3×10^{-7} mbar and the ionization time = 75 ms.

indeed improved as is demonstrated by Fig. 9(a), which shows the spectrum obtained for n-butylbenzene under optimized conditions. Ions at *m/z* 91 and *m/z* 92 are nearly baseline resolved as is observed in the expanded scale of Fig. 9(b). The simulation, shown in Fig. 9(c), predicts even better resolution although, again, space charge effects were not considered in the simulation. Additional mass spectra from benzene (Fig. 10) and perchloroethylene (Fig. 11) using the asymmetric toroidal analyzer support the demonstrated improvement in mass resolution.

The resonance ejection point used to acquire these data corresponds to the hexapole resonance at β eject = 2/3. This results in narrow peaks, but due to the nonlinear radial fields, it can be expected to be the cause for strong loss of ions in the radial direction, once the radial ion oscillation frequency matches the applied resonance excitation frequency. In addition, the ionization times used in the experiment are long compared to ionization times used in commercial ion traps. The result may be a large number density of trapped ions. Even if a significant portion of the ions were ejected in the radial direction, the large overall ion number density still leads to a sufficient number of ions ejected axially (to the detector). Therefore, space charge effects may be limiting the current resolution of the device. Additional simulations (not shown) predict that the application of a quadrupolar dc potential to the trap to separate the radial and axial ion oscillation frequencies may reduce ion loss due to radial ejection, thereby allowing a lower ion abundance to be detected. This experiment requires additional, unavailable hardware and as such must be the subject of future investigations.

Acknowledgements

Funding for this work was provided by the U. S. Department of Energy Office of Research and Development (NN-20), Chemical and Biological Nonproliferation Program (CBNP). Oak Ridge National Laboratory is managed and operated by UT-Battelle, LLC, for the U. S. Department of Energy under Contract No. DE-AC05-00OR22725. S.A.L would like to acknowledge R. Graham Cooks (Purdue University) for his support of this effort by providing the custom data-input programs for POISSON and an unreleased, beta version of the ITSIM program.

References

[1] Practical Aspects of Ion Trap Mass Spectrometry, J.F.J. Todd, R.E. March (Eds.), CRC Press, Boca Raton, 1995, Vol. 1–3.
[2] K.J. Hart, M.B. Wise, W.H. Griest, S.A. Lammert, Field Anal. Chem. Technol. 4 (2000) 93.
[3] J.A. Syage, B.J. Nies, M.D. Evans, K.A. Hanold, J. Am. Soc. Mass Spectrom. 12 (2001) 648.
[4] R.T. Short, D.P. Fries, M.L. Kerr, C.E. Lembke, S.K. Toler, P.G. Wenner, R.H. Byrne, J. Am. Soc. Mass Spectrom. 12 (2001) 676.
[5] W. Plass, Int. J. Mass Spectrom. 202 (2000) 175.
[6] E.R. Badman, R.C. Johnson, W.R. Plass, R.G. Cooks, Anal. Chem. 70 (1998) 4896.
[7] E. Fischer, Z. Phys. 156 (1959) 1.
[8] J.E. Fulford, D.N. Hoa, R.J. Hughes, R.E. March, R.F. Bonner, G.J. Wong, J. Vac. Sci. Technol. 17 (1980) 829.
[9] J.M. Campbell, B.A. Collings, D.J. Douglas, Rapid Commun. Mass Spectrom. 12 (1998) 1463.
[10] J.D. Prestage, G.J. Dick, L. Maleki, J. Appl. Phys. 66 (1989) 1013.
[11] P.T.H. Fisk, M.A. Lawn, C. Coles, Appl. Phys. B 57 (1993) 287.
[12] M. Schultz-Johanning, R. Schnabel, M. Kock, Eur. Phys. J. D 5 (1999) 341.
[13] M. Bier, J.E.P. Syka, U.S. Patent No. 5, 420, 425 (30 May 1995).
[14] J. Dress, W. Paul, Z. Phys. 180 (1964) 340.
[15] D.A. Church, J. Appl. Phys. 40 (1969) 3127.
[16] I. Waki, S. Kassner, G. Girkl, H. Walther, Phys. Rev. Lett. 68 (1992) 2007.
[17] M. Aramaki, Y. Sakawa, T. Shoji, Jpn. J. Appl. Phys. 39 (2000) L246.
[18] J.E.P. Syka, A.E. Schoen, Int. J. Mass Spectrom. Ion Processes 96 (1990) 97.
[19] U. Steiner, U.S. Patent No. 5, 559,327 (24 September 1996).
[20] P.H. Dawson, N.R. Whetten, Int. J. Mass Spectrom. Ion Phys. 2 (1969) 45.
[21] J. Franzen, R.-H. Gabling, M. Schubert, Y. Wang, in Practical Aspects of Ion Trap Mass Spectrometry, J.F.J. Todd, R.E. March (Eds.), CRC Press, Boca Raton, 1995, Vol. 1, Chap. 3.
[22] D. Gehrlich, in State—Selected and State-to-State Ion Molecule Reaction Dynamics, Part 1: Experiment, C.-Y. Ng, M. Baer (Eds.), Wiley, New York, 1992.
[23] O. Chun-sing, H.A. Schessler, Int. J. Mass Spectrom. Ion Phys. 35 (1980) 305.
[24] J.E.P. Syka, in Practical Aspects of Ion Trap Mass Spectrometry, J.F.J. Todd, R.E. March (Eds.), CRC Press, Boca Raton, 1995, Vol. 1.

[25] P.H. Hemberger, N.S. Nogar, J.D. Williams, R.G. Cooks, J.E.P. Syka, Chem. Phys. Lett. 191 (1992) 405.
[26] Quadrupole Mass Spectrometry and Its Applications, P.H. Dawson, (Ed.), Elsevier, Amsterdam, 1976; reprinted by American Institute of Physics Press, Woodbury, 1995.
[27] J.M. Wells, W.R. Plass, G.E. Patterson, Z. Ouyang, E.R. Badman, R.G. Cooks, Anal. Chem. 71 (1999) 3405.
[28] J.M. Wells, W.R. Plass, R.G. Cooks, Anal. Chem. 72 (2000) 2677.
[29] F. Guidugli, P. Traldi, A.M. Franklin, M.L. Langford, J. Murrell, J.F.J. Todd, Rapid Commun. Mass Spectrom. 6 (1992) 229.
[30] J. Franzen, Int. J. Mass Spectrom. Ion Processes 130 (1994) 15.
[31] J.H. Billen, L.M. Joung, Proceedings of the 1993 Particle Accelerator Conference, 1993, p. 790.
[32] Y. Wang, J. Franzen, Int. J. Mass Spectrom. Ion Processes 132 (1994) 155.
[33] H.A. Bui, R.G. Cooks, J. Mass Spectrom. 33 (1998) 297.
[34] W.R. Plass, J.M. Wells, R.G. Cooks, Proceedings of the 48th ASMS Conference on Mass Spectrometry and Allied Topics, Long Beach, CA, 2000, p. 1572.
[35] W.R. Plass, Thesis, Universität Giessen, 2001.
[36] J. Louris, J. Schwartz, G. Stafford, J. Syka, D. Taylor, Proceedings of the 40th ASMS Conference on Mass Spectrometry and Allied Topics, Washington, DC, 1992, p. 1003.